Hall D Forward Drift Chamber Prototype Test Plan

August 4, 2003

Daniel S. Carman
Department of Physics
Ohio University
Athens, OH 45701, USA

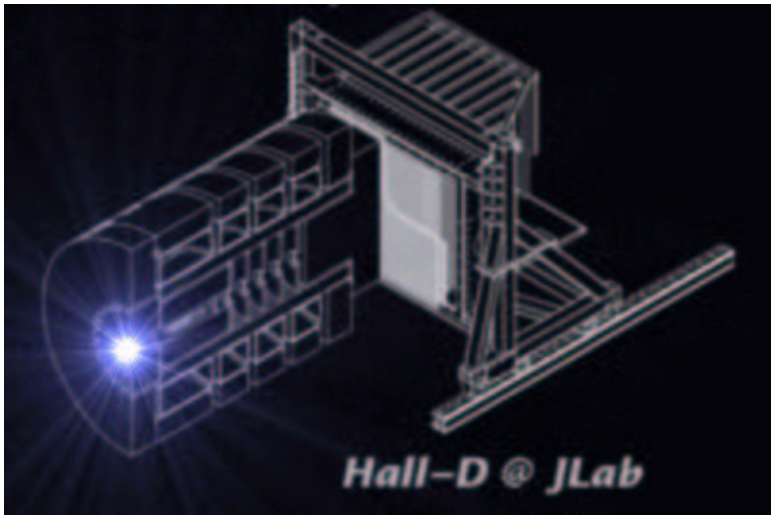

Contents

Abstract

This document represents a compendium of information regarding the Hall D Forward Drift Chamber prototype. It also includes a test plan for the full slate of studies for the prototype. The different studies planned are discussed along with the steps required to carry them out. This document is expected to evolve and expand as the test plan is carried out and the detector design work continues. Errors and omissions should be sent to the author at carman@jlab.org.

1 Introduction

Fig. 1 is a schematic representation of the proposed HALL D detector. This facility is being optimized in its design to study photon-nucleon interactions leading to final states where multiple charged and/or neutral particles can be present. The detector consists of a large superconducting solenoid magnet whose inner volume is filled with a target, tracking chambers, and calorimeters. The magnet is employed to bend charged particles emerging from the beam-target interaction region into helical paths. By reconstructing the trajectories of these charged particles via the use of tracking chambers as they move through the detector, their momenta can be accurately determined. The calorimeters are used to determine the energy of both charged and neutral particles. The solenoid will be followed by further "downstream" detector systems used to measure the energies of the scattered particles to aid in particle identification. This hermetic system will allow for complete reconstruction of the final states of the photon-nucleon interaction. The superconducting solenoid magnet was originally part of the LASS spectrometer at SLAC and was later moved to LANL for the MEGA experiment.

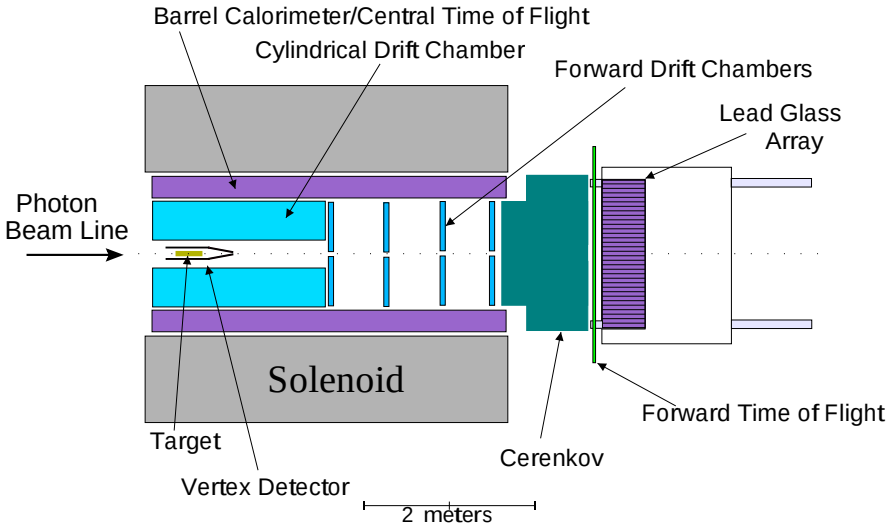

Figure 1: Schematic overview of the HALL D detector. The main detector subsystems, including the solenoid magnet, the calorimeters, and the elements of the drift chamber tracking system are identified.

Within the solenoid, the Forward Drift Chambers (FDCs) represent the main system for charged-particle track reconstruction between the target region and the downstream detector systems [1]. In the current detector design, the FDCs include four separate sets of disk-shaped planar drift chambers to measure the momenta of all charged particles emerging from the target at angles of up to 30° relative to the photon beam line. Each set of the four FDCs is envisioned to be identical.

The basic FDC drift package is a plane of wires with 150 μm spatial resolution between two planes of cathode strips. By charge interpolation of the electron avalanche image charge in the cathode strip readout, spatial resolutions at the cathode planes are expected of roughly 100 μm. The strips are arranged in a U and V geometry with respect to the wires (at $\pm 45°$),

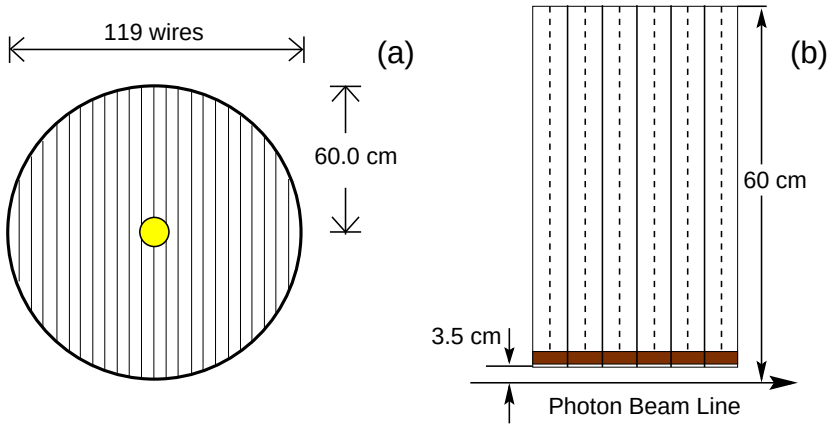

Figure 2: Schematic views from the front (a) and side (b) of a single FDC package. In (a) the wires are schematically indicated as the vertical lines. In (b) is shown a side view of the upper half of an FDC package with the wire planes shown as the dashed lines.

allowing the reconstruction of a 3–D space point from each hit. The chambers are arranged in packages of six to provide a small track segment to facilitate later linking of tracks. Given the number of spiraling tracks, it is critical that these chamber packages not only provide good spatial resolution but also reasonable direction information.

The basic chamber element is a disk of outer radius 60.0 cm, where the wires are strung as chords across the chamber as shown in Fig. 2(a). With a 1.0 cm wire spacing, each chamber will contain 119 wires. In addition, there will be an equal number of cathode strips on each face. This leads to 357 channels per chamber element. Fig. 2(b) shows the six chamber elements in side view forming one FDC package, leading to about 2150 channels per package. Adjacent chamber elements will be rotated by 60° with respect to each other to improve the overall resolution. The wires that cross through the beam line will be deadened out to a radius of about 3.5 cm to reduce the otherwise unmanageable rates.

The primary development issues associated with the FDCs that must be addressed are factors affecting the intrinsic resolution of the chambers, along with the mechanical and electronics layout. The goal is to construct a tracking detector that meets the required design specifications and has a long life time, a uniform and predictable response, a high efficiency, and is serviceable in case of component failure.

2 Cathode Strip Chambers

The material in this section borrows heavily from the following references:

- ATLAS Technical Design Report Chapter 6, June 1997.
- H. Fenker *et al.*, "Precision Interpolating Pad Chambers", NIM A **367**, 285 (1999).
- PHENIX Collaboration, PHENIX Internal Note PN125.

2.1 Introduction

Cathode strip chambers (CSCs) are typically multiwire proportional chambers (MWPCs) with a symmetric drift cell in which the anode-cathode spacing d is equal to the anode wire pitch S (see Fig. 3).

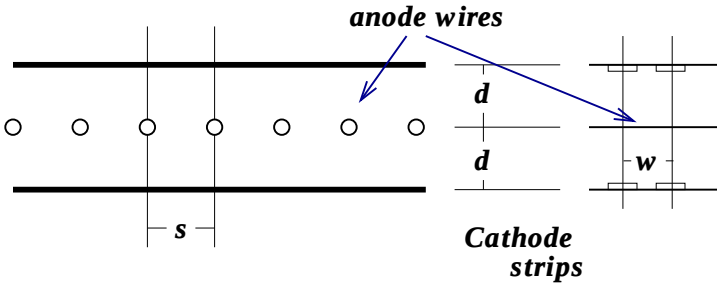

Figure 3: Schematic diagram of a generic cathode strip chamber.

In a typical MWPC, only the anode wire hits are read out, which limits the spatial resolution to $\approx s/\sqrt{12}$ (RMS). In a CSC the precision coordinate is obtained by measuring the charge induced on the segmented cathode by the avalanche formed on the anode wire.

The optimum cathode readout pitch w is determined by the width of the charge distribution and the desire to keep the number of readout channels to a minimum while maintaining a linear response. It has been shown in Ref. [5, 6] that minimal differential non-linearity ($\approx$1%) is achieved when w/d is near unity. In the FDC prototype w/d=0.5 mm/0.5 mm=1.

Simulations from Ref. [3] have shown that resolutions of 25 μm could be achieved for minimum-ionizing tracks if the electronics and readout could be provided with noise and inter-channel gain variation less than 0.5% of the nominal pulse height.

In the FDC prototype tests we will not be able to define an incident track with such resolution, and we certainly can only hope to provide electronics and readout inter-channel gain variations on the few percent level.

2.2 Spatial Resolution

In a CSC the precision coordinate is obtained by a relative measurement of charges induced by the avalanche on adjacent cathode strips. Therefore modest (<20%) variations in the gas gain of the chamber do not affect the spatial resolution. For this reason the CSC performance

is relatively immune to variations in temperature and pressure commonly encountered in the laboratory or experimental hall. Since no precision time measurement is involved in a generic CSC detector, the operation is insensitive to the drift properties of the operating gas.

The primary factor limiting the CSC spatial resolution is the electronic noise of the preamplifier. The precision in the determination of the center-of-gravity of the induced charge depends linearly on the signal-to-noise ratio. Eventually other factors, such as uncertainty in the electronic gain calibration and geometrical cathode distortions, set the limit for this technique at about 25 μm.

Following the arguments of Ref. [2], if we assume that the projection of the avalanche position on the cathode strip plane is at a point x=0, then the position of the center-of-gravity is given by the ratio of the first and second moments of the charge distribution on the strip plane via:

$$x_{c.g.} = \frac{\sum_{i=1}^{N} x_i q_i}{\sum_{i=1}^{N} q_i}, \tag{1}$$

where x_i=iW and W is the pitch of the cathode readout. If the charges q_i are measured with an RMS error of σ, then the uncertainty in $x_{c.g.}$ is given by:

$$\sigma_{c.g.} = \frac{\sigma}{Q}\sqrt{2\sum_i x_i^2} \tag{2}$$

or

$$\sigma_{c.g.} = \frac{\sigma}{Q}\sqrt{2W^2 + 2(4W^2) + 2(9W^2) + \ldots}. \tag{3}$$

Therefore the resolution depends on the number of strips used. Monte Carlo simulations show that the optimum number lies between three and five strips. The resolution deteriorates rapidly for one or two strips (not enough information), while it increases slowly when more than five strips are used because the electronic noise of more channels is added in quadrature.

It is also important to note that the optimal CSC resolution is obtained when the cathode strips are perpendicular to the anode wires. In this arrangement there is no quantization of the position measurement resulting from the discrete nature of the anode wires. However, CSCs are typically used to measure a three dimensional space point on a track by rotating the opposing cathode plane strips at an angle with respect to each other.

2.3 Track Reconstructions

Resolution degradation of the CSCs comes primarily from two sources, tracks inclined from the normal to the face of the chamber and Lorentz angle effects. In both cases the spatial resolution is degraded because the deposited charge is distributed non-uniformly along the anode wire due to the energy loss fluctuations in the gas. The charge interpolation is optimum when the avalanche is formed on a single point on along the wire. A finite spatial extent of the anode charge results in a resolution degradation $\mathcal{D}$. Studies of the PHENIX CSCs have shown that $\mathcal{D}$ goes as:

$$\mathcal{D} = 0.16d\tan\theta, \tag{4}$$

where $2d$ is the cathode-to-cathode spacing and θ is the angle from the normal to the face of the chamber.

Such non-local charge distributions can be caused by a number of factors, including δ electrons, inclined tracks, and a Lorentz force along the anode wire in the presence of a magnetic field that is not collinear with the electric field of the chambers. It should be noted (see Ref. [2]) that the Lorentz effect in a CSC does not result in a systematic shift of the measured coordinate. It does not, therefore, require a correction. It simply degrades the resolution because of the spread of the charge along the wire.

From the analysis in Ref. [3] it has been shown that there is no significant loss of resolution when two charged tracks are very near to each other such that their charge distributions overlap. Their findings indicate that the spatial resolution for tracks separated by less than one pad width is degraded by less than a factor of five. When the tracks are separated by two or more pad widths, the nominal single track resolution is achieved.

3 FDC Prototype Overview

The FDC prototype chamber has been designed primarily to provide us experience with cathode strip chambers. Through detailed study of this prototype we hope to be able to better understand which electrode structure and layout will fulfill the design requirements for the final Hall D FDC chambers. The prototype will also provide important insights into the mechanical design, tolerances, construction and assembly techniques, noise immunity, and calibrations that will be important for the final FDC detector design. Some of the elements of the FDC prototype design have descended from the cathode chambers employed in the original LASS spectrometer [7].

A cartoon of the FDC prototype chamber is shown in an exploded view in Fig. 4. The basic chamber layout consists of two cathode planes with strips oriented at $\pm 45^\circ$ sandwiching a single wire plane. The gas volume is defined by two outer aluminum frames that each include an aluminized mylar window. The active area of the prototype chamber is roughly 20 cm $\times$ 20 cm, and the chamber is about 8 cm thick. The full set of mechanical drawings for the FDC prototype chamber is included in Appendix I.

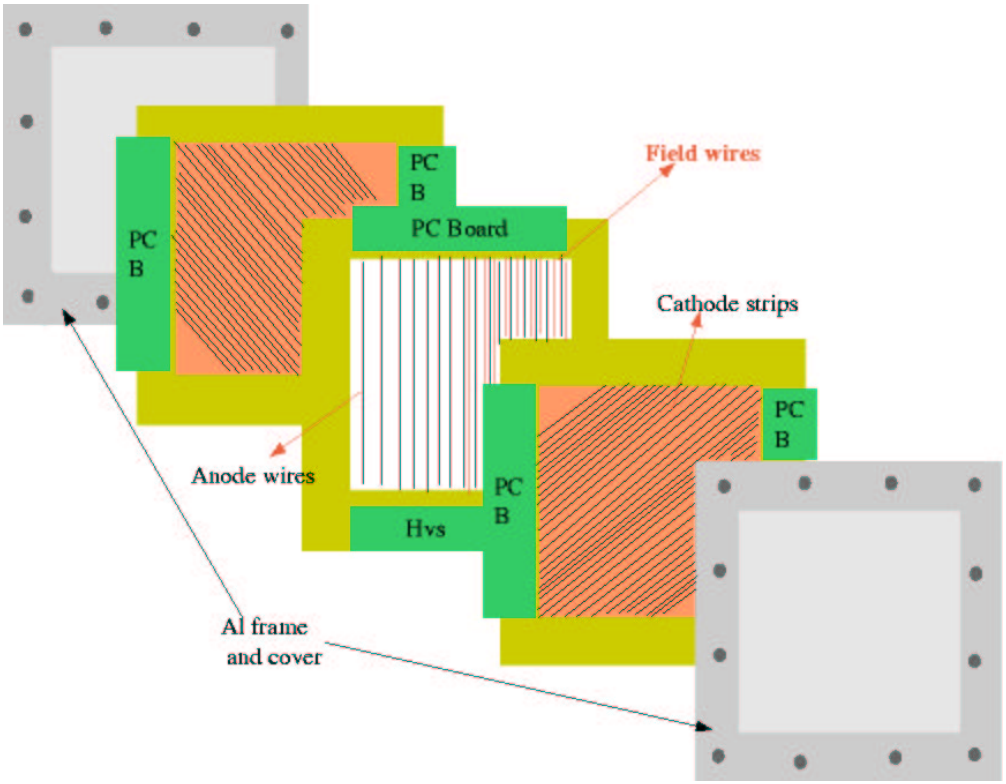

Figure 4: Cartoon representation of the FDC prototype chamber in an exploded view showing the wire plane, two cathode planes, and the two aluminum window frames.

The layouts of the wire plane and the cathode planes are shown in Fig. 5. The 1.5-mm thick G10 (fiberglass) wire frame contains both sense wires and field wires. The U and V cathode planes are mirror symmetric with respect to each other. The cathode planes are copper-clad kapton sheets ($\sim$20 mil thickness) mounted onto 5-mm thick G10 frames. The

chamber is designed to operate with the sense wires at positive high voltage, the field wires at negative high voltage, and the cathode strips at ground.

The printed circuit board for the wires was designed to capacitively decouple high voltage from the signals and to route the signals to the output connector. The printed circuit board for the cathodes routes the signals directly to the output connector. Not shown on the boards in Fig. 5 are the small signal routing circuit boards (SRCBs) that attach to the output connectors on the wire and cathode circuit boards. These SRCBs contain the preamplifiers for each readout channel. The output will connect to a twisted-pair line that will route the signals to the readout electronics. The SRCBs used for the cathode readout are different than those for the wire readout in order to account for the polarity difference in these signals.

Each readout channel has its own associated "SIP" preamplifier. These single-channel transimpedance preamplifiers were originally designed for the Hall B CLAS detector [8]. They have complementary outputs designed to amplify signals by a factor of 2.25 mV/μA. Besides high gain, characteristics of the SIPs include: fast rise and fall time (3 to 4 ns), wide frequency bandwidth, wide dynamic range, and low noise and power dissipation (65 mW). The power requirement for a single SIP is 5 VDC at 13 mA, and is supplied by a low-voltage power supply.

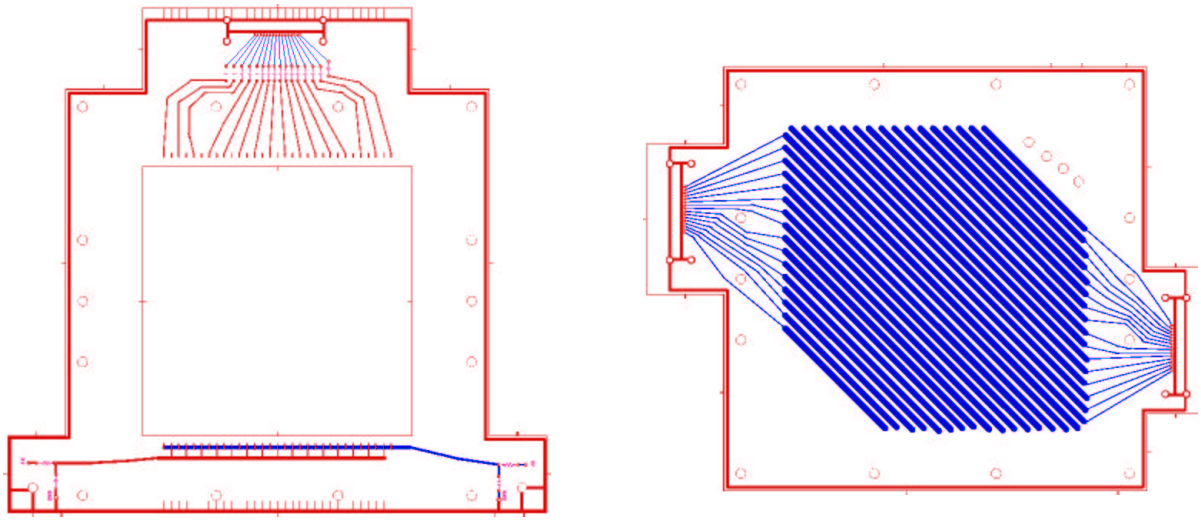

Figure 5: Left: Schematic drawing of the wire frame showing the signal traces at the top and the high voltage busses at the bottom. Right: Schematic drawing of the cathode plane showing strip readout on either side.

The wire plane was designed to consist of two distinct electrode structures. One half of the plane will be instrumented with only sense wires and the other half will include both sense and field wires. The purpose of the different electrode structures is to understand the trade-offs between timing resolution from the wire planes and spatial resolution from the cathode planes. In total the chamber includes 16 sense wires, separated by 1 cm. In the half of the wire plane including the field wires, they will be separated from the sense wires by 0.5 cm. The cathode planes are located 5 mm away from the wire plane. They each include 32 copper strips with a pitch (or center-to-center separation) of 5 mm. Three different sets of U and V cathode planes have been designed with strip separations of 0.25 mm, 0.50 mm,

and 1.00 mm to allow for the optimal configuration to be determined. The circuit board electronics layouts for the sense, field, and cathodes are shown in Fig. 6.

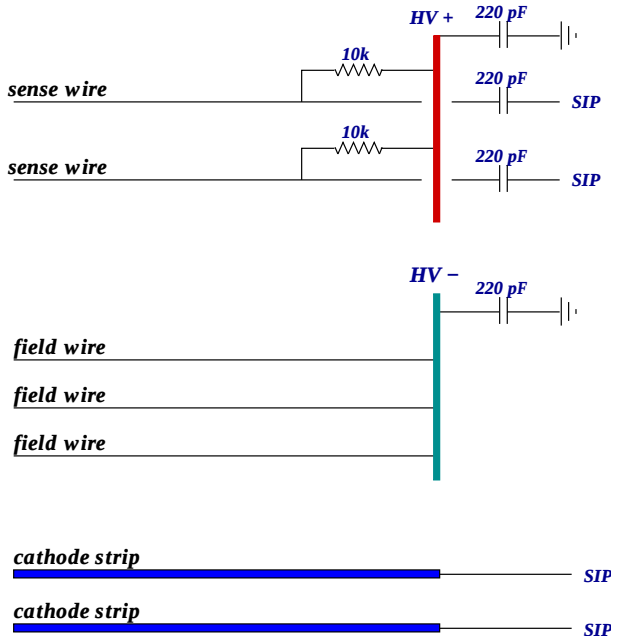

Figure 6: Circuit board electronics for the sense and field wires, along with the cathode strips.

In Section 4 of this document is included a formal test plan for the FDC prototype. The test plan is divided into four major sections or phases. These include:

i). Prototype Assembly
ii). Benching Testing
iii). Resolution Studies
iv). Miscellaneous

• The *Prototype Assembly* section focusses on cleaning procedures for the circuit boards, wire winding, prototype assembly, and alignment of the different chamber pieces.

• The *Bench Testing* section focusses on first-order prototype check out. This includes studies of shorts, gas leaks, high voltage conditioning, voltage plateau, operational stability, noise pickup, cross talk, and checkout of individual channels. It also includes studies of different chamber gas mixtures and measurements of the chamber gas gain.

• The *Resolution Studies* section includes details on the studies to measure the prototype resolution under a number of different conditions. This work will be carried out using a cosmic ray test stand with wire chambers on loan from the STAR group at IUCF. Details regarding the test stand are given in Section 5. Another important aspect of this portion of the test plan is to come to an understanding of the optimal electrode structure for the final FDC design, balancing the trade-off between timing resolution from the wire planes and spatial resolution from the cathode planes.

• The *Miscellaneous* section includes a series of other studies of importance for the prototype such as deadening portions of the sense wires along the photon beam line and techniques for chamber alignment, positioning, and support. There are also studies involving noise susceptibility and operation in a magnetic field environment.

4 Prototype Test Plan

This section details the important steps in the prototype assembly, testing, and measurement. It is important throughout each step in the test plan to keep a very detailed log of what is being done. This documentation should include as many relevant photographs as necessary.

4.1 Prototype Assembly

4.1.1 Chamber Cleaning and Materials

To minimize potential voltage break down effects due to arcing or discharge, all chamber pieces must be cleaned prior to assembly to remove any surface oils or films that may have been introduced during the machining or construction. It is also true that this is essential practice to minimize the effects of chamber aging, although aging considerations are usually not critical for prototype chambers. However, when it comes to wire chambers, it is good practice to try to ensure that all materials in contact with the gas volume are clean and "chamber safe" as defined in Ref. [9]. It is also not clear at this time if the chamber construction and assembly should be carried out in the JLab clean room or not, however, this too is usually a good practice if sufficient space is available. Note: In our Hall B chamber experience, three different types of epoxy were used in areas exposed to the chamber gas. Shell Epon resin 826 mixed with Versamid 140, and Scotchweld varieties 210 and 2216 were employed. These mixtures have been studied extensively and found not to outgas significantly [10]. All flexible gas tubing should be polyflo, avoiding nylon whenever possible.

In construction of the Hall B drift chambers, all metal parts were cleaned to remove machining and finger oils employing a Micro-laboratory detergent from the Cole-Parmer Instrument Company. This should also be used for the fiberglass (G10) spacers, frames, and circuit boards, which are usually machined without any lubricating oils. Immediately prior to chamber assembly all pieces should undergo a cleaning procedure consisting of (in sequence), cleaning with detergent, de-ionized water, and alcohol, and then blown dry with pure nitrogen gas.

Any questions regarding chamber cleaning procedures can be directed to Steve Christo or George Jacobs at JLab who have extensive experience in this area.

4.1.2 Wire Plane Stringing

To limit wire tensions and operating voltages, the wire diameter has to be minimized. The sense wire for all chambers will consists of 20-μm diameter gold-plated tungsten, the smallest practical choice. Tungsten is chosen because of its durability, and the gold-plating of the wires (of thickness 0.127 μm) ensures chemical inertness as well as a smooth surface finish. The expected electronics gain and thresholds for the chamber readout dictate that the gas gain be a factor of a few times 10^5. Under this condition, the electric field at the surface of the sense wires is $\approx$280 kV/cm. The field-wire diameter is chosen to ensure that the electric field at their surface remains below 20 kV/cm to minimize conditions causing cathode deposits [9, 11]. Since there are two field wires for each sense wire (in the half of the chamber instrumented with both), this requires that the diameter of the field wires be about seven

times the diameter of the sense wire. The field wire for all chambers consists of 140-μm diameter gold-plated aluminum. Aluminum is chosen because it has the longest radiation length of any practical wire material and thus minimizes multiple scattering. Additionally, the low density of aluminum means that the field wires can be strung at lower tension than a more dense wire, with minimal gravitational sag. This minimizes the forces on the 0.157-cm thick G10 wire frame.

The present plan is to string the wire plane using using the wire winding table provided by Howard Fenker of JLab. Howard has agreed to provide instruction for the use of this system, as well as a demonstration of the operation. The chamber will be strung with 16 sense wires separated by 1 cm. One half of the chamber will be strung with 8 field wires separated by 1 cm, with 0.5 cm separation from the sense wires.

The appropriate values for the sense and field wire tensions are not fully defined at this time. Estimates are in the neighborhood of 30 gm of tension on the sense wires and 100 gm on the field wires. The total force on the wire frame from the 16 sense wires and 9 field wires (with these nominal tensions) is then 13.5 N (=3.0 lbs). The effect of this load on the thin wire frame needs to be carefully studied to minimize warping effects. It may be necessary during the wire stringing process to clamp the wire frame onto a stiff backing board until it is ready to be incorporated into the final prototype chamber assembly.

The actual wire-winding procedure is relatively straightforward and can be described by the following steps:

i). Wind the sense and field wires onto the winding table. In this process only one wire type can be wound at a time. Care will have to be taken to accurately define the offsets between the sense and field wires. Note that the winding system itself is fully automated and computer-controlled. The interaction is mainly during threading of the wire into the machine, setting the wire tension properly, and watching over the winding process to ensure smooth operation.

ii). After the wires are wound on the table, place the wire frame under the wires so that they are in direct contact. Line up the frame with the wires using the fiducial marks at the top and bottom of the frame as a guide. Fig. 7 shows a schematic representation of the winding table with the wire frame positioned under the wires.

iii). Place epoxy glue strips just above and just below the opening in the wire frame to fix the locations of the wires. Note that the wires can be individually epoxied to avoid the necessity of glue strips if deemed more appropriate. Allow the epoxy several hours to set up.

iv). Solder the wires to the solder pads on both sides of the wire frame opening.

v). Cut the wires just at the top of the solder pads using an X-acto knife. This completes the wire winding process.

4.1.3 Wire Plane Checks

Once the wire plane has been strung, it is important to ensure that the wire separations and positions are known. It is also important to ensure that the wires are parallel. Any wires that are strung outside of allowed positioning tolerances will have to be re-strung. For

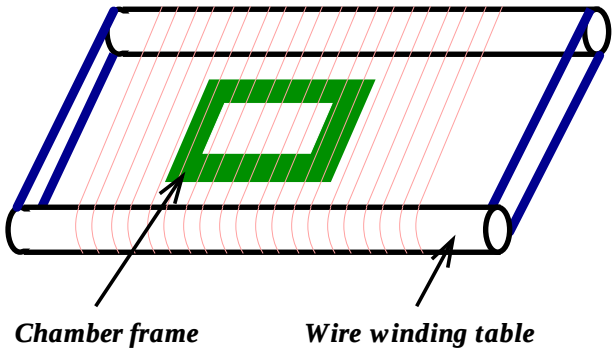

Figure 7: Schematic drawing of the wire winding table strung with wires and the wire frame positioned under the wires.

the prototype, this tolerance is not fully clear, but a reasonable value is 100-200μm. The precision in the placement of the wires is important for the generation of a uniform electric field, which ensures the best possible resolution on the spatial resolution in the cathode plane measurements. The measured wire positions can also be included in the reconstruction software to achieve the best possible spatial resolution for the charged particle tracks.

In order to measure the positions of the wires on the frame, a lathe table in the JLab shop has been outfitted with a camera. The wire plane is attached to the table, and the position of the table can be recorded precisely when a wire is located by the cross-hairs on the camera. Steve Christo is responsible for this equipment and has volunteered to be available for assistance in setting up the measurements.

To ensure that the wires are parallel and to study the skewing of the wires, the measurements should be repeated at the top and bottom of the wire frame. The outermost wires must also be located with respect to the external frame fiducial marks (located on either side of the output connector) in order for the wire positions to be known once the chamber is fully assembled (and the wires are no longer visible).

I do not expect that there should be major problems with the wire tension settings for either the sense or the field wires with the small prototype board. However, a scheme can be setup using a magnet, an AC frequency generator, and an oscilloscope to measure the wire tensions via detection of resonant frequencies. The process is described in Appendix II.

At this stage the quality of the cathode plane can also be assessed. Using the same optical system described above to measure the locations of the wires on the wire frame, the uniformity and spacing of the cathode strips should be studied. These features are crucial in order to achieve the optimal resolution.

4.2 Assembly

The FDC prototype contains 9 layers, made up from the two aluminum windows, four G10 spacers, two cathode planes, and the G10 wire frame. Each layer contains two precision dowel-pin holes located on opposite sides to fix the alignment of each layer relative to each other during the assembly process.

Before the prototype assembly begins, the gas windows must be attached to the alu-

minum window frames. The windows will be constructed from aluminized mylar. The exact thickness is not crucial, but 10-20 μm thicknesses are appropriate. The window material should be attached to the outside of the aluminum frame using double-sided tape. The aluminum layer on the window material should face outward and be grounded via copper tape to the frame to form a proper ground shield.

The next step is to solder the 10 $k\Omega$ resistors and the 220 pF capacitors to the wire plane in the appropriate configuration. Fernando Barbosa will be able to supply the components. The excess length of the component leads should be cut off. The signal connectors can be attached next to the wire plane and the cathode planes. Note that at the present time, the attachment of the connectors to the SRCB boards has not been thought out in great detail. This was not viewed as a major issue during the prototype design, but a final scheme will have to be devised. Finally the HV connectors must be attached to the wire frame circuit board.

The assembly process itself starts by placing one of the window frames face down onto an assembly jig. Care must be taken to ensure the mylar windows are not in contact with the table top to avoid pin holes in the thin window material. Two dowel pins (of length $\approx$2.5 in are then inserted into the window frame. Each subsequent layer in the stack assembly is then placed on the previous layer in the proper order, relying on the dowel pins for proper alignment.

The gas seal between the chamber layers will be accomplished through the use of 1/8" and 3/32" o-rings (see Appendix I mechanical drawings). In order to ensure the o-rings don't fall out of the o-ring grooves, they can be tacked in with epoxy at the corners and middles. Note that there is no gas seal between the cathode planes and their associated G10 frames. If gas seals are a problem here, then the cathode planes can be epoxied to the G10 frame. For each cathode plane that is part of the prototype, there should be one corresponding G10 spacer board.

After the chamber stack assembly is completed, four bolts are inserted into the corners to compress the o-rings and seal the chamber. Care should be taken not to over-tighten the bolts as the o-rings could be damaged. The final step in the process is to attach the signal routing circuit boards (SRCBs) to the wire plane and the cathode planes.

The mechanical stability of the assembled prototype needs to be studied in detail as uniformity in the spacing between all chamber layers is crucial to maintain to optimize performance. Care must also be taken with the wire plane during prototype construction as the wire load should be expected to cause the plane to warp. However, we also expect that after assembly of layers of the full prototype, no warping will be detectable. The situation for the full scale FDC chambers can be expected to be much different due to the different physical size and the increased number of wires. This will be studied in due time. It may be necessary in the future to consider including internal chamber supports for the wires and/or cathode planes to ensure the configuration does not change under mechanical load or under voltage.

4.3 Bench Testing

4.3.1 Short Checking Level I

The first level of bench testing with the completed prototype is to look for undesired shorts between channels. This work should be done with a DVM. Ensure that all channels from the wire plane and cathode planes are not shorted to each other, to the high voltage busses, or to ground. Also ensure that the high voltage busses are not shorted to each other or to ground. It is important to make all necessary ground connections (and make sure that they are robust) to minimize noise.

At this point high voltage can be applied to the sense and field wires at the level of a few hundred volts (even before connecting the chamber to gas) to check for evidence of high resistance shorts. Further studies of high resistance shorts will be carried out with the prototype in a proper gas environment.

Finally, the preamplifiers on the wires and the cathode strips should be connected to power. Any problems in terms of high resistance shorts or noise pickup on the wires or cathodes should be fully investigated.

4.3.2 Gas Flow

The chamber should be connected to a gas handling system for the next phase of the checkout. The initial gas mixture should be 90% Argon - 10% CO_2. The mixing can be done initially using vernier style flow meters (see Fig. 8) or the gas can be supplied from a pre-mixed calibration gas. The gas flow should be set to the minimum level for bubbles to appear in the output mineral oil bubbler. The chamber should be reasonably leak tight at this point. If there are clear signs of leaks, the reason must be determined and repairs made.

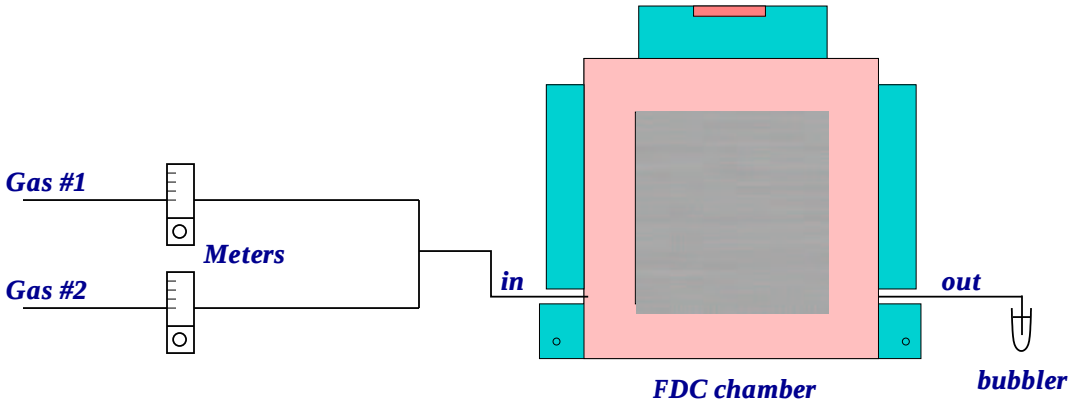

Figure 8: Schematic illustration of the gas connections to the FDC prototype chamber.

For the precision tests of the chamber in Section 4.4, it may be necessary to use electronic flow meters to better control the gas mixture if the mixing is done using separate gas bottles. It is also not clear what gas mixture will be employed for the resolution studies. Argon-CO_2 is chosen to start with as it is non-flammable and has a fairly high saturated drift velocity (> 4 cm/μs). This mixture typically has an operating voltage plateau of several hundred

volts before breakdown occurs. We can expect reasonable efficiency, adequate resolution, and reasonable collection times.

Other gas mixtures may prove more adequate in terms of collection times and noise immunity. We won't know the answer until the prototype chamber reaches this stage in the testing. If a flammable gas mixture is deemed necessary, special procedures will need to be enacted for safety reasons. Elton Smith and the JLab Safety office will need to be consulted for guidelines.

4.3.3 Short Checking Level II

The next stage in the bench testing procedure is to work to bring the chamber up to full voltage. The wire plane has been designed to hold voltage up to +1500 V on the sense wires and -750 V on the field wires. However, until the voltage plateau is completed for the gas mixture employed, the nominal operating point is unknown (although it can be crudely determined looked at the SIP output through a VPI postamplifier).

As the voltage on the wires is increased toward the upper bounds, two important operations will be completed simultaneously.

i). The chamber wire plane will undergo high voltage conditioning. In the process, the positive corona discharge on the sense wires is allowed to burn off dust and other impurities in the vicinity of the wires.

ii). Further studies of the electrostatic stability of the chamber can be carried out and high impedance shorts and high voltage breakdown areas can be investigated. Any problems discovered must be repaired at this stage.

Note that chamber conditioning can only proceed as fast as the leakage currents measured on the high voltage supply will allow. Leakage currents should be allowed to rise no higher than $\approx$10 μA. Sustained current draws much higher than this can lead to sparks (which can break wires in some cases) or can lead to carbon deposits in unwanted places (leading to breakdown and noise).

4.3.4 High Voltage Plateau Scans

When the chamber conditioning is completed, a series of high voltage plateau studies need to be completed in order to study the prototype efficiency and to determine the best voltage setting for operation

Fig. 9 shows how the measurements should be set up, sandwiching the prototype between two thin plastic scintillators (S1 and S2). Here cosmic rays that pass through the detector stack are studied. The chamber efficiency definition is given by:

$$\epsilon = \frac{S1 \cdot S2 \cdot N_{wire}}{S1 \cdot S2}, \tag{5}$$

where the numerator represents the number of coincidences between a given wire and the two scintillators in a narrow time window and the denominator represents the number of coincidences between only S1 and S2. The required electronics setup for the readout is shown

in Fig. 10. Notice that the efficiency measurements employ visual scalers to determine the numerator and denominator of eq.(5).

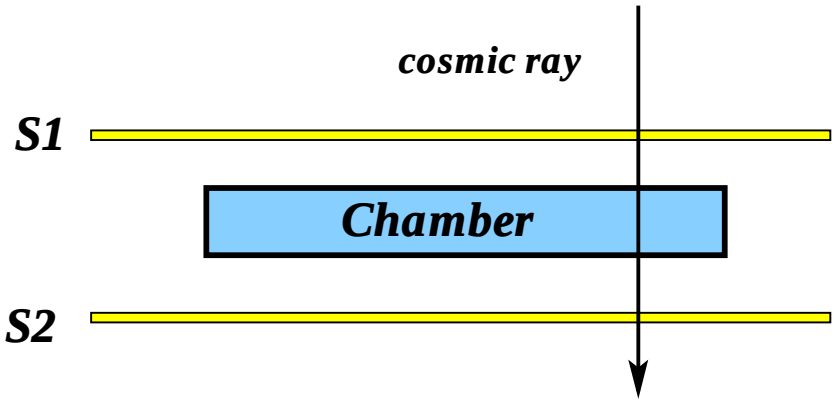

Figure 9: Detector set up to be employed for the plateau scans showing a cosmic ray track passing through the detectors. Here S1 and S2 are scintillators.

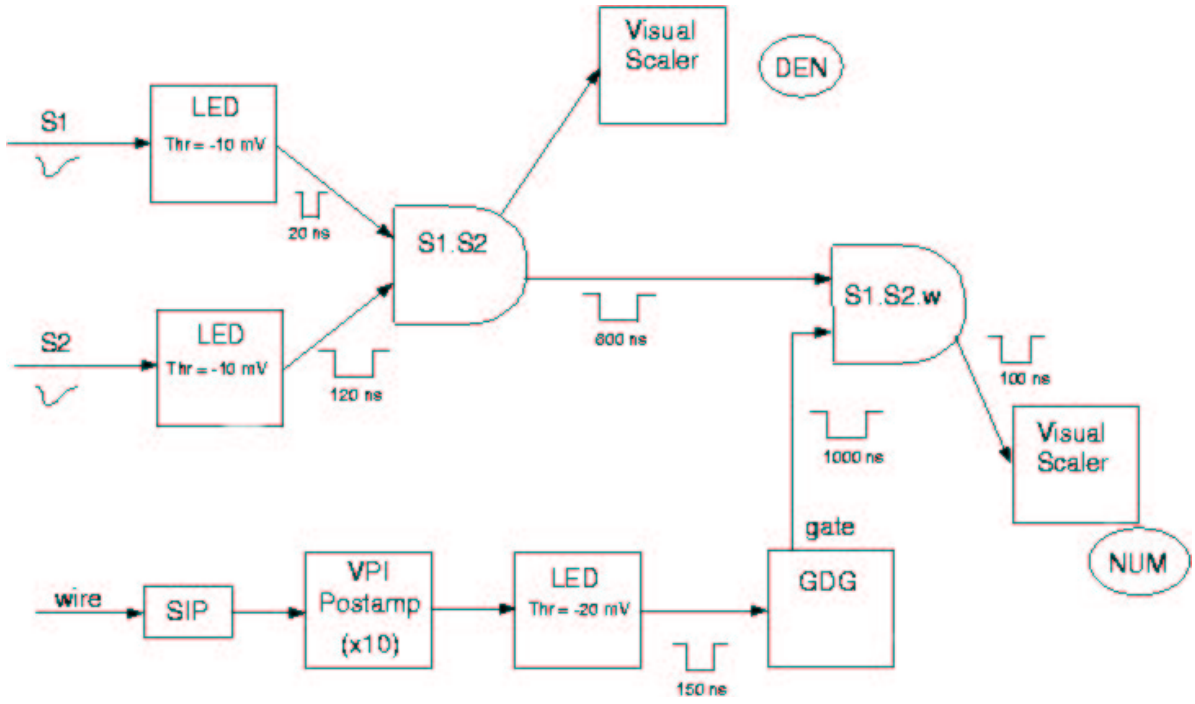

Figure 10: Example of the electronics set up for the prototype plateau scan.

The plateau scans should be done for several wires on both halves of the wire plane. As the electrode structure is different for the two sides of the wire plane, we should fully expect that the efficiency plateau points will be different. We can also expect that the drift cells on the boundary between the two halves will not be fully efficient when the chamber is at operating voltage due to a non-ideal electric field configuration.

The plateau studies should proceed by setting a fixed value for the field wire voltage (e.g. -500 V, -600 V, -700 V) and increasing the sense wire voltage. At each setting for the

field wire voltage, a plateau scan for the sense wire efficiency should be completed. It is important to take sufficient measurements around the "knee" of the voltage plateau curve to fully characterize its shape. It is also important to measure the full voltage plateau region (see Fig. 11). The single wire efficiency should be in excess of 95-98%, accounting for differences in the scintillator sizes relative to the drift cell size. Note that in Fig. 11, the relevant quantity to plot is the voltage difference between the sense and field wires in the chamber half instrumented with both wire types, and the relevant quantity in the other half of the chamber is the sense wire voltage.

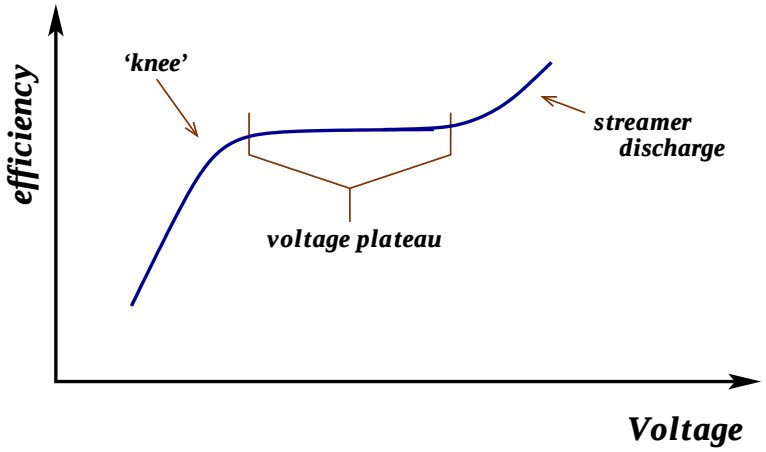

Figure 11: Representative efficiency vs. voltage curve for a drift chamber.

The operating point for the chamber should be safely above the knee so that variations in atmospheric pressure do not alter the chamber efficiency. However, the operating voltage should be set as low as possible to minimize electrostatic instabilities and to ensure the chamber remains in the proportional regime. A full plateau study will have to be performed for each different gas mixture employed during the prototype testing in order to determine the appropriate settings for efficient chamber operation.

4.3.5 Gas Gain Measurements

Measurements of the prototype gas gain can be performed for each chosen gas mixture employing an ^{55}Fe source. This will produce 5.9 keV γ rays. As shown in Fig. 12, the output of the sense wire can be taken directly into the Q-input of a QVT (no amplification through a SIP or a postamplifier). The horizontal and vertical outputs of the QVT should be connected to a fast oscilloscope operated in X-Y mode. The oscilloscope then will show a two dimensional representation of the number of counts versus the collected charge. The QVT should be gated internally with a gate width set to about 200 ns. The QVT threshold should be set to reduce the noise at levels ranging from -1 mV (at the lowest gains) to -10 mV (at the highest gains). Given the measured channel of the peak of the 5.9 keV γ rays in the QVT charge spectrum along with the conversion gain of the QVT, the gas gain can be determined as:

$$G = \frac{QVT \text{ channel} \cdot G_{QVT}}{Q_e \cdot N_{Fe}}. \tag{6}$$

Here G_{QVT} is the selected conversion gain of the QVT (in pC/channel), Q_e is the electron charge, and N_{Fe} represents the number of electrons liberated from the 5.9 keV γ ray, a number that is gas mixture dependent. Typical values are 200 - 250.

In this procedure the gas gain is measured directly from the wire. The output is not taken from the SIPs to remove the uncertainty in the current-dependent gain from these preamplifiers. The gas gain should be roughly 10^5.

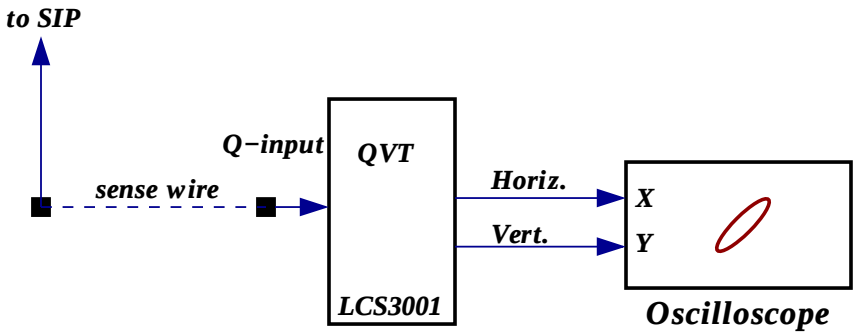

Figure 12: Electronics configuration for the drift cell gain measurements using the QVT method.

4.3.6 Noise Measurements

Electronic noise on the wire and cathode signals is not necessary a problem endemic to the prototype chamber. In many cases noise and cross talk arise due to non-optimal shielding and grounding configurations and can be mitigated to a large extend with some careful detective work. Depending on the level of the noise and cross talk in the prototype testing environment, work may have to be done to reduce the levels so that they do not adversely affect the results of the tests. Of course, if the problem is due to some design flaw in the prototype, we need to identify what the root cause is due to.

The noise level on the different readout channels can be characterized by looking at the output of the different readout channels at the output of the SIP passed through a postamplifing stage. With the DC offsets removed, the noise level can be defined as the oscilloscope threshold necessary such that less than 10% of the triggers are due to noise, where noise pulses should be discernible by their characteristic pulse shape.

4.4 Resolution Studies

The main goal of the resolution studies is to determine the position resolution for charged tracks that pass through the chamber. There are position resolutions associated with both the wire plane and the cathode plane. We can expect the position resolution within the chamber to depend on where the charged track passes through the chamber. This arises due to the different electrode structures in the two halves. The resolution will also depend on the angle of the track relative to the wire plane.

Of course the wire plane was designed with two distinct halves precisely in order to allow us to determine which electrode configuration gives the best resolution. A schematic diagram of the two halves of the wire plane is given in Fig. 13. Fig. 14 shows GARFIELD [12] calculations of the electric field lines for these two different electrode configurations in a 90% argon - 10% CO_2 gas mixture with no magnetic field present.

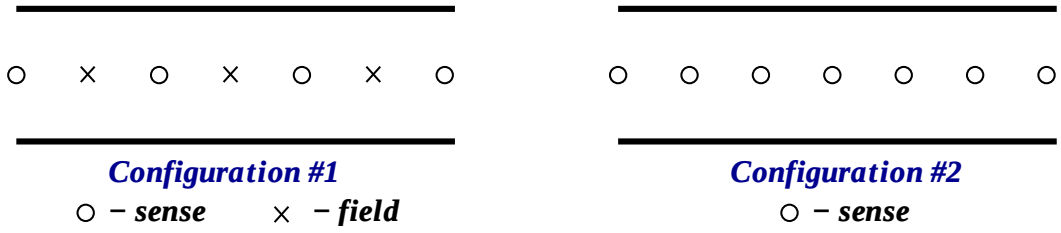

Figure 13: Schematic drawing of electrode structure in the two halves of the FDC prototype.

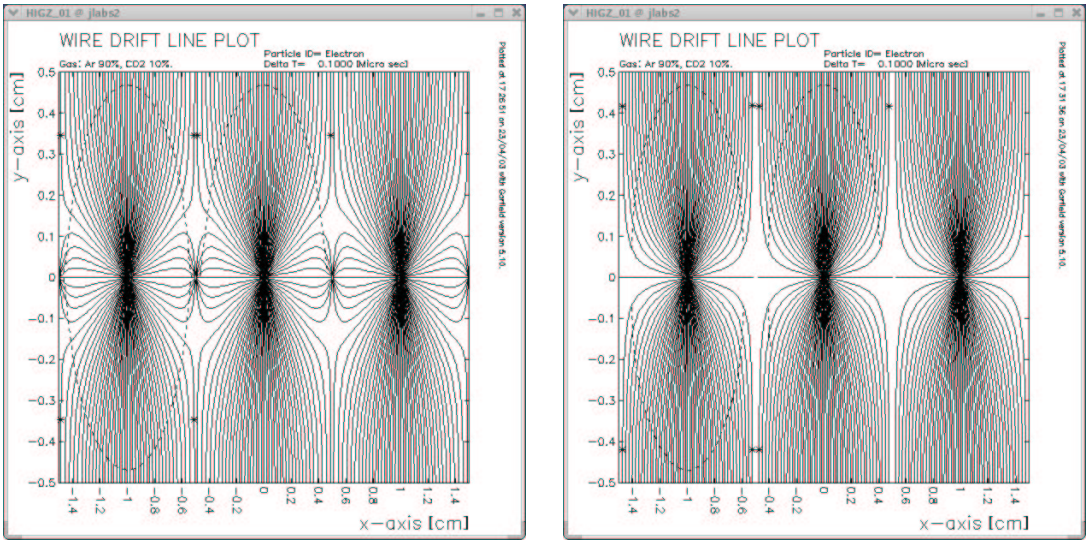

Figure 14: Plots of electric field lines for a 90% argon - 10% CO_2 gas mixture for the two electrode configurations in the FDC prototype.

The principles of operation of a horizontal drift chamber (like the FDC prototype) are such that the best position resolution is achieved when the first electrons that reach the sense wire drift along field lines in the plane of the wires. For field configurations like that on the right side of Fig. 14, the first electrons to reach the sense wire will most certainly

arise from other locations. This gives rise to a non-linearity in the space-time correlation. It is clear from Fig. 14 that that drift time resolution in the portion of the chamber with no field wires will be much worse than in the portion with the field wires present. The affect on the cathode position resolution is not known. The FDC prototype was designed to better understand the trade-offs between the timing resolution in the wire plane and the position resolution in the cathode plane. In typical cathode chambers (or interpolating pad chambers), the main purpose of the wires is to generate the uniform electric field within the drift volume (see discussion in Section 2).

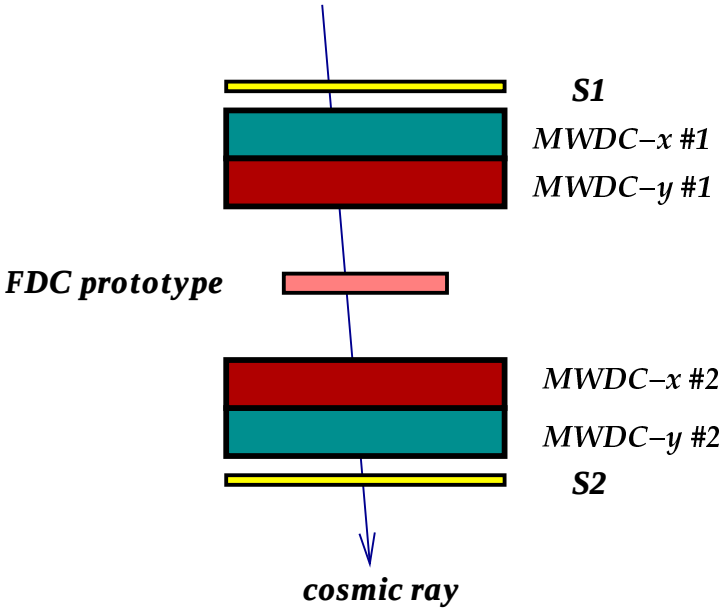

Figure 15: Schematic drawing of the cosmic-ray telescope to be used for resolution studies.

4.4.1 Cosmic Ray Telescope

In order to perform precision measurements of the spatial resolution of the wire plane and cathode planes of the FDC prototype, some calibrated external detectors must be in position to precisely define the passing charged particle. For our purposes we will employ a cosmic ray telescope (see Fig. 15). This system employs multiple layers of drift chambers above and below the test chamber to precisely define the trajectory of an incident track that can be compared against the positions measured in the FDC prototype layers for comparison.

Here the upper and lower drift chambers (MWDCs) each have multiple layers in both x and y. The scintillators above and below the chambers ($S1$ and $S2$) are used to provide the electronics and data acquisition system trigger. The coincidence signal between $S1$ and $S2$ also provides the common start to the drift chamber TDCs and the gate to the ADCs for the cathodes. More details regarding the cosmic ray telescope for the FDC prototype studies will be included in Section 5 when details become available. However, the cosmic test stand must be able to define a track with a resolution of better than 200 μm at the FDC prototype.

Note that the discussion in Section 2 makes it clear that cathode chambers have the

potential to provide position resolutions better than 100 μm. As the design goal for the FDCs is position resolutions on the order of 150 μm (see Section 1), it may ultimately be necessary to study the FDC prototype in a test stand with more accurate tracking detectors (e.g. silicon strip chambers). However, a moderate resolution testing stand should be adequate for our initial studies.

In order to provide the required accuracy for the resolution studies, the chambers in the test stand (and the prototype itself) must be properly calibrated. After the chamber alignment (described in the next section), the drift time to drift distance calibrations must be determined. A simple way of measuring the space-time relationship in a drift chamber is to record its time spectrum (see Fig. 16 for an example) in a uniformly distributed beam. In fact,

$$\frac{dN}{dt} = \frac{dN}{ds}\frac{ds}{dt} = kv_d(t). \tag{7}$$

Therefore the time spectrum represents the drift velocity as a function of the time of drift, and its integral the space-time relationship. The limitation of this method lies in the accuracy with which a uniform incident flux can be produced over the active area of the chambers.

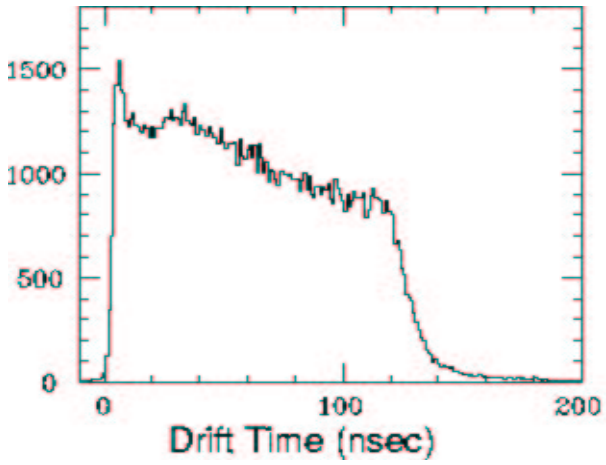

Figure 16: Representative drift time distribution for a typical horizontal drift chamber with a similar electrode layout to the FDC prototype.

The steps in the calibration are then simply:

- Apply timing offsets t_{off} for each channel to align the drift time spectra such that t_{min} is at zero.
- Integrate the drift time spectrum from t_{min} to t_{max}. Call this value INT_{full}.
- Integrate the drift time spectrum bin-by-bin from t_{min} to t_{bin}. Each of these values are called INT_{bin}.
- A lookup table can then be created with the values INT_{bin}/INT_{full} for each bin in drift time.

- The TDC value (or bin value) for a given measurement can then be converted to a drift distance using INT_{bin}/INT_{full} times the drift cell size.

The calibration can be optimized by studying the fit residuals ($x_{meas} - x_{calc}$) in the multi-layer fit. Changes in t_{off} can be made to center the residual distributions about zero. Distributions of the drift distance vs. fit residual will be rotated if t_{max} is set too high or too low.

4.4.2 Single Track Resolution Studies

The technique to determine the FDC prototype position resolution is relatively straightforward in principle. The cosmic ray test stand is used to define a track through the prototype chamber that can be compared against the information in the chamber. Fits to the relevant distributions, $x_{cosmic} - x_{fdc}$ (wire plane), $U_{cosmic} - U_{fdc}$ (U cathode plane), and $V_{cosmic} - V_{fdc}$ (V cathode plane), summed over many events, provide the answers. Of course this measurement requires some care.

1). The layers of the cosmic ray test stand (e.g. MWDC-x #1,2 and MWDC-y #1,2 in Fig. 15) must be properly aligned with respect to each other. Fiducial marks on the test stand chambers should be used to perform the initial drift cell alignments. Finally, special normal-incidence triggers can be defined to check alignments.

2). The FDC prototype chamber must be aligned within the test stand. During the wire plane checks (see Section 4.1.3), the positions of the wires in the wire plane should be referenced to the external fiducial marks on the wire plane. The positions of the individual cathode strips can be determined relative to these fiducial marks due to the tight alignment set by the dowel pins.

The information from the geometry measurements must also be properly included in the tracking software. After the alignment of the drift cells in the test stand, again special normal-incidence triggers can be employed to check the alignment of the FDC prototype relative to the test stand. Of course this stage of the test plan requires that the associated DAQ system is functioning to readout the timing and hit information from the test stand chambers, along with the timing, hit, and pulse height information from the prototype chamber.

Once the alignment and calibration have been completed, the main studies of interest are resolution measurements of the wire plane and cathode planes channel-by-channel as a function of the incidence angle of the charged track. These studies will have to be carried out in two stages as the operating point (plateau bias) for the two halves of the FDC prototype will undoubtedly be different. Keep in mind that the width of the difference distributions: $x_{cosmic} - x_{fdc}$ (wire plane), $U_{cosmic} - U_{fdc}$ (U cathode plane), and $V_{cosmic} - V_{fdc}$, which are related to the prototype resolution, also include the resolution of the track defined by the test stand, i.e. $\sigma = \sqrt{\sigma^2_{cosmic} + \sigma^2_{fdc}}$.

A schematic layout of the readout electronics for the resolution measurements is provided in Fig. 17. A Linux box to be used for the DAQ has been moved into the EEL building at JLab (contact Elliot Wolin) (RedHat 7.3.14 installed). The system already has CODA

installed on it for data acquisition. Presently a FASTBUS crate for the ADCs and TDCs is not in-hand. When this is procured, the DAQ system can be fully configured.

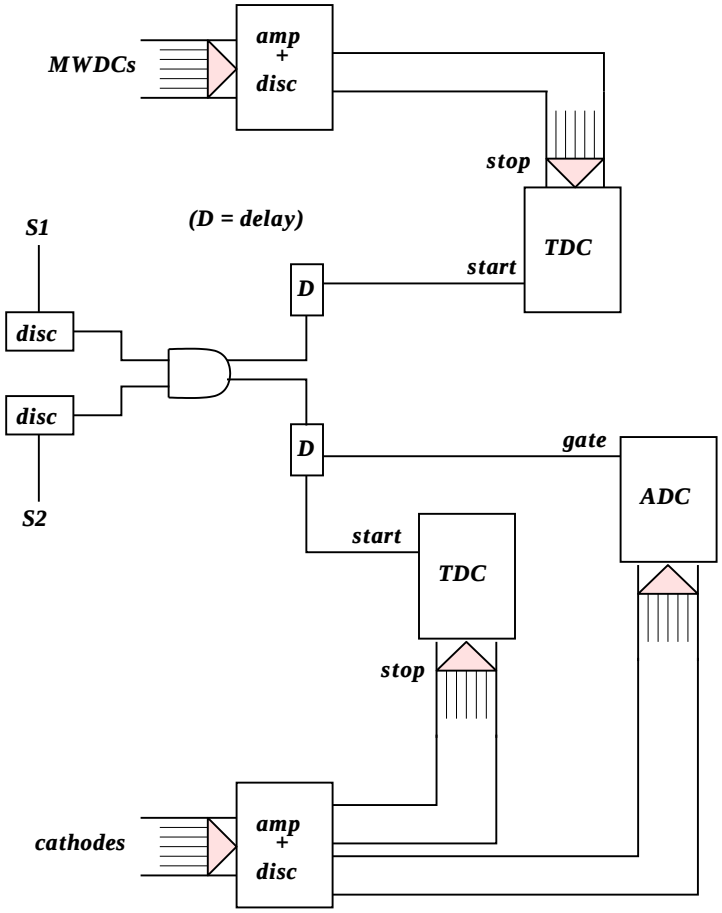

Figure 17: Schematic layout of the readout electronics for the resolution measurements.

4.4.3 Chamber Efficiency

The test stand configuration can also be employed to study the prototype efficiency wire-by-wire and strip-by-strip. The procedure is to look at the prototype hit information for all tracks defined by the test stand. The efficiency can also be studied as a function of the angle of incidence of the charged track.

4.4.4 Two Track Resolution

For events where two cosmic tracks have been included within one readout window (coincidence overlap between $S1$ and $S2$), the efficiency for separating two tracks can be investigated. The test setup will not be ideal for these studies as the probability of two tracks having overlapping ion charge distributions at the cathode plane will be low. It is also possible that the resolution of the FDC prototype will be comparable to that of the track defined by the test stand. As such, detailed studies may have to wait.

4.4.5 Cross Talk Measurements

The ideal way to study cross talk (electronic pickup) between neighboring channels is to be able to pulse the channels with an external, controllable source. As we will not have that ability with the prototype chamber we will have to investigate other methods. No great deal of thought has been put into the design of such studies at this time. One technique could be to employ an ^{55}Fe source with tight collimation directed at a single wire. Then neighboring channels could be readout looking for correlated signals as a function of the discriminator threshold setting.

4.5 Miscellaneous

4.5.1 Magnetic Field Studies

The final FDC chambers will operate within the solenoid magnet in a region of large magnetic fields. The solenoid can be expected to have a very uniform magnetic field (of order 2 Tm) in the majority of its volume. It can also be expected to become non-uniform as we approach the coils. The affect of such strong magnetic fields on the operation of the chambers in general, and on their associated resolution will need to be investigated in detail.

4.5.2 Wire Center Deadening

As discussed in Section 1 the wires in the FDC that cross the beam line will be deadened out to a radius of 3.5 cm to reduce the otherwise unmanageable rates due to the primary photon beam. Several techniques have been suggested to accomplish this, including packing styrofoam about the wires, and epoxying mylar or polyurethane to the cathodes. Schemes involving different "chamber safe" materials and different attachment techniques can be studied in the FDC prototype.

4.5.3 Noise Pickup in RF Environment

The final FDC chambers will ultimately operate in the harsh RF environment of the HALL D experimental area. The chamber operation and noise immunity must ultimately be investigated in such an environment. It is possible that the prototype chamber could be employed for such studies if it could be operated parasitically in one of the operating JLab Halls.

4.5.4 Alignment and Positioning

Several important issues ultimately need to be tackled regarding the alignment and positioning of the full complement of FDC chambers. Typical schemes employ a self-aligning rail system for the positioning and alignment of chambers. This rail system will slide into and out of the solenoid magnet. The system must also allow support all gas, high and low voltage cables, and signal cables associated with the FDC detector (and possibly others as well). It must be designed such that the entire set of chambers can be inserted and removed without unplugging any cables. The chambers must be able to operate in both the "in" and "out" configurations. It is also important that individual chambers be accessible for servicing and/or removal when required.

4.5.5 Chamber Internal Supports

Due to the important of maintaining a fixed half-gap size (the distance between the cathode planes and the wire plane) and the size of the full FDC chamber ($\approx$1 m in diameter), schemes may have to be incorporated into the final design to add supports to fix this dimension. The original LASS cathode chambers [7] incorporated such a support scheme.

5 Cosmic Ray Test Stand

I have negotiated with the STAR group at IUCF to borrow a complement of wire chambers to employ as a cosmic ray test stand at JLab. The chambers were originally employed at Fermilab in a neutrino experiment. The complement includes 19 chambers made from extruded aluminum. Each detector has a cross section as shown in Fig. 18 and is 1 m in length. Inside each chamber there are 15 cells, 8 over 7, offset by one half a cell spacing. Each cell is 1 in $\times$ 1 in with a single anode wire running down its length.

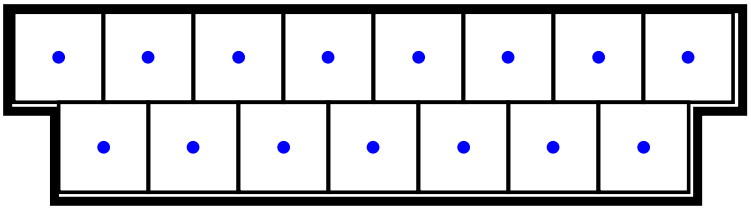

Figure 18: Cross section of one of the extruded aluminum Fermilab chambers. Each 1 m long chamber is 8 in wide by 2 in high.

The chambers were transported to JLab in July 2003. After they were unpacked, they were fully re-conditioned and setup in the EEL building in the configuration shown in Fig. 19.

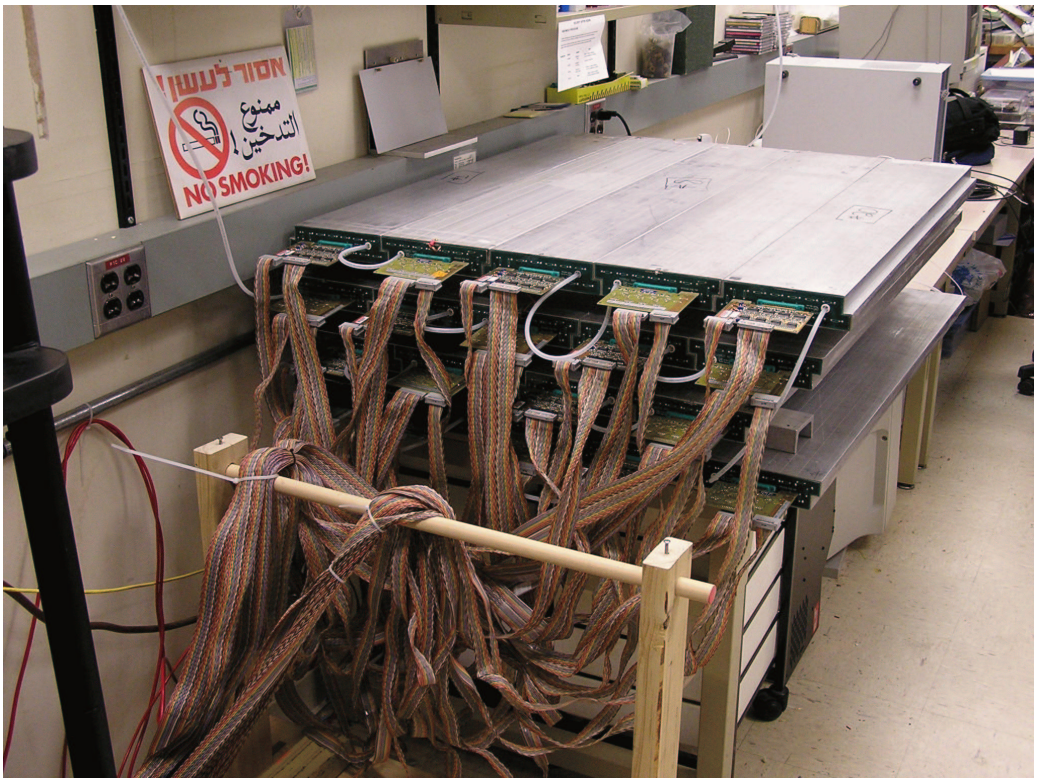

Figure 19: Cosmic ray test stand currently set up in the EEL building at JLab.

The readout is accomplished using chamber-mounted 2735DC and 2735PC preamplifier-discriminator cards. The chamber conditioning was accomplished using a 90% Argon - 10% CO_2 gas mixture. A crude plateau was completed showing the chambers started to become efficient at $\sim$-2100 V. The discriminator threshold was set at -3.5 V. The studies will completed without bubbling the chamber gas through propanol as the folks at IUCF advised (none was available at the time of our initial studies).

Appendix I – FDC Prototype Mechanical Drawings

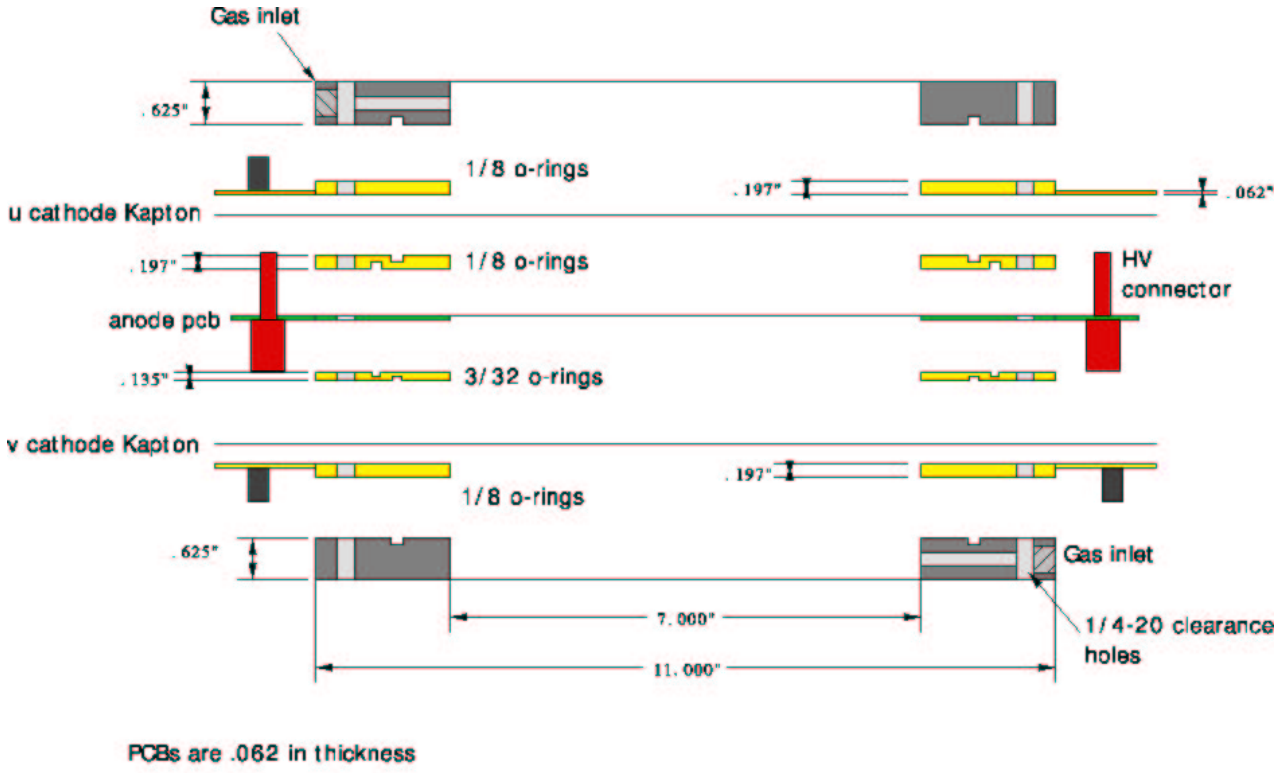

Figure 20: View of the FDC prototype chamber with the wires running into and out of the page.

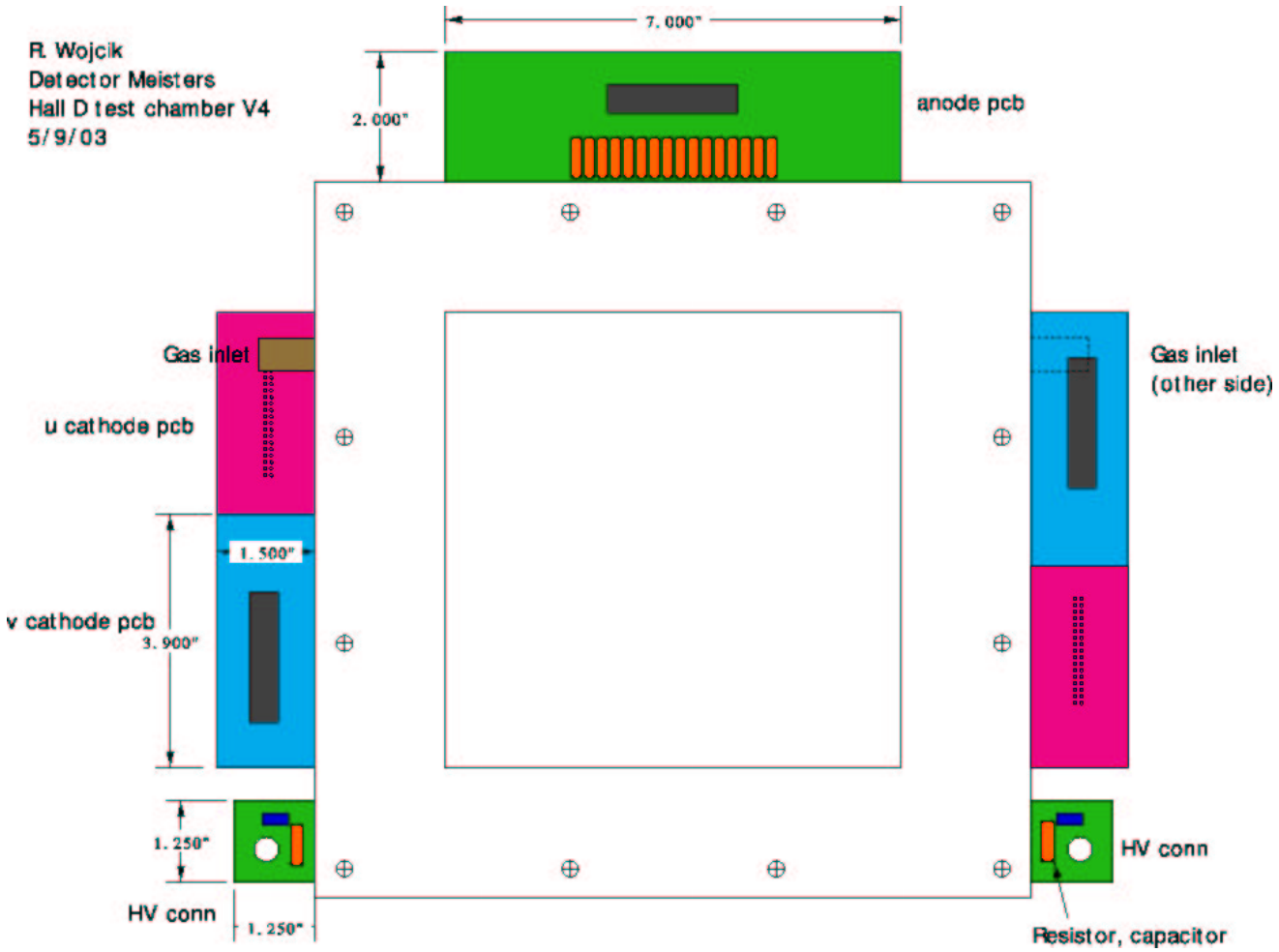

Figure 21: Front view of the FDC prototype chamber.

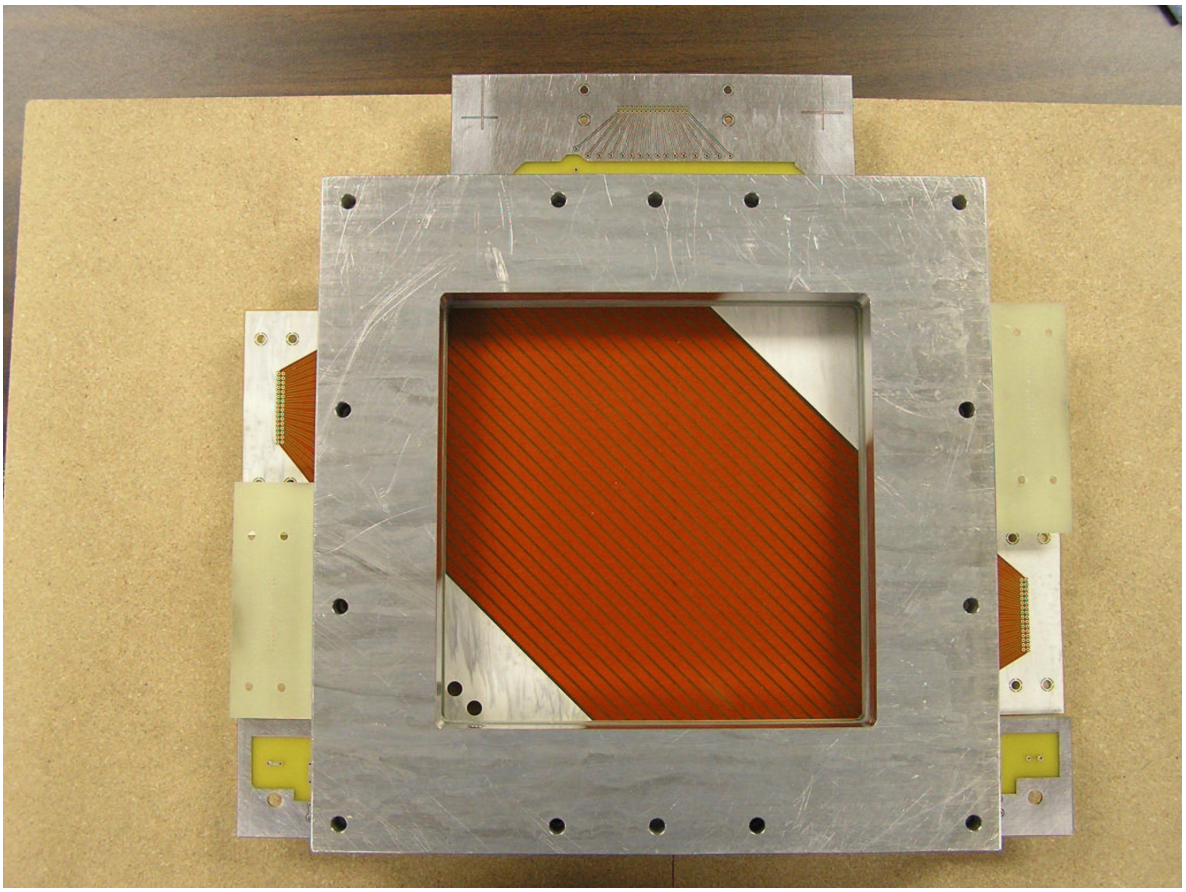

Figure 22: Front view of the FDC prototype chamber with the actual prototype pieces before assembly began.

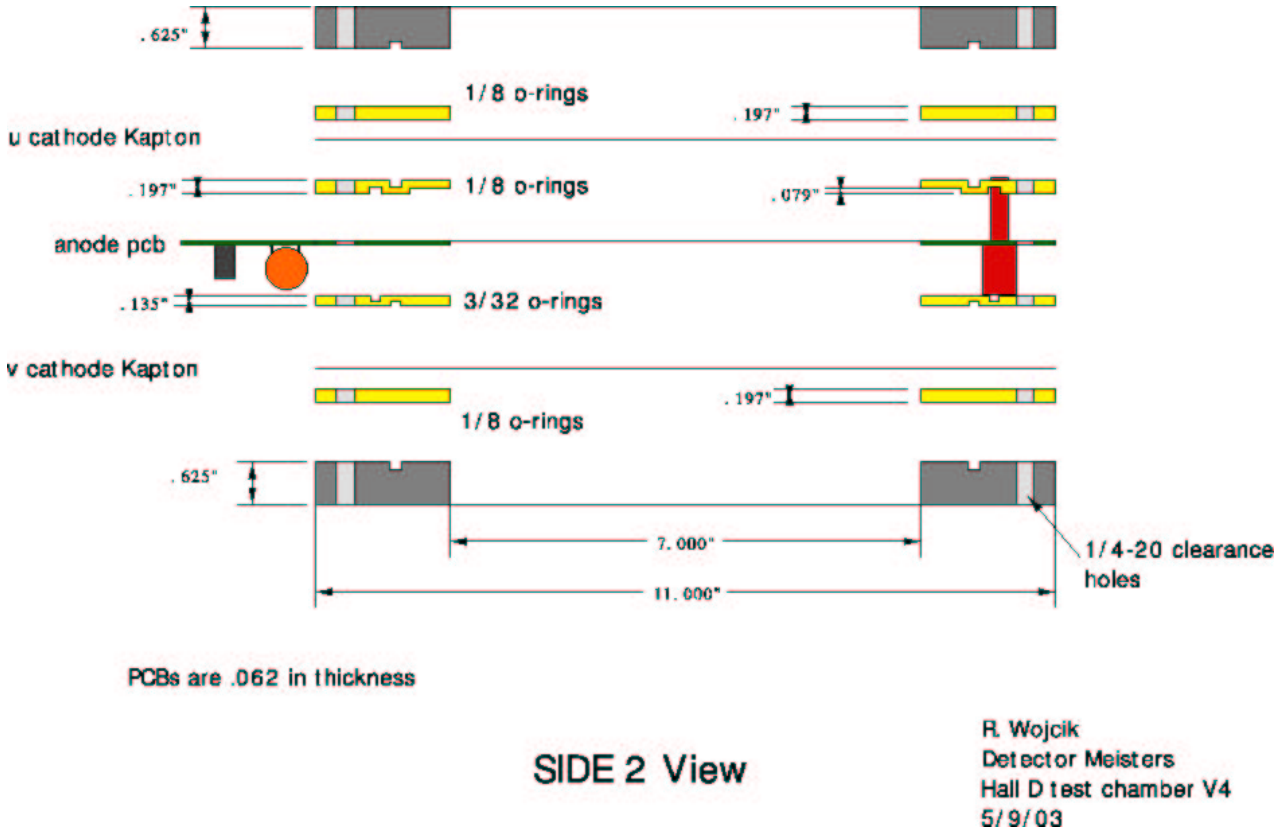

Figure 23: View of the FDC prototype chamber with the wires running in the plane of the page.

Appendix II – Wire Tension Measurements

Wire tensions can be measured via the magnetic induction of resonant frequencies. A basic illustration of the different components is shown in Fig. 24. Here the AC generator drives the wire as some trial frequency and the response is measured on the oscilloscope. The driving force should be generated by a sinusoidal current of ≈30 mA (RMS) in a magnetic field of ≈20 G. The response is due to the EMF induced in the wire as it oscillates in the magnetic field, i.e. the wire vibrating in the magnetic field produces an induced voltage with an amplitude of ≈ 1 mV.

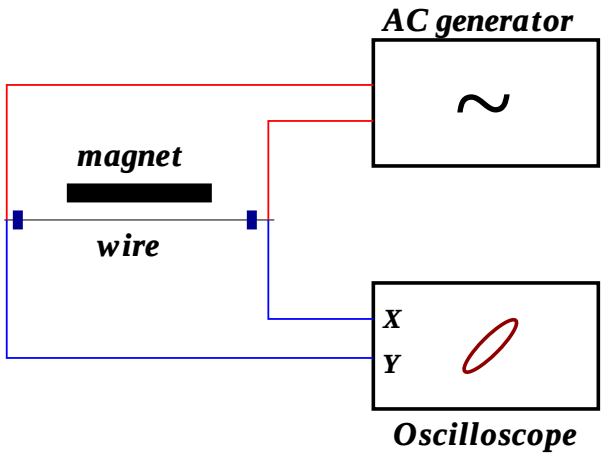

Figure 24: Schematic layout of the setup that can be used to measure the tension in a wire via magnetic induction of resonances.

The layout of the magnet relative to the wire will dictate which harmonic resonances can be induced in the wire. An even magnetic field across the entire wire generally excites only the fundamental frequency. Uneven magnetic fields allow harmonics with n=1,3,5,etc. The wire tension T can be computed by:

$$T = \frac{4}{g} L^2 f^2 \mu, \tag{8}$$

where T is in grams if the wire length L is in meters, the fundamental frequency f is in Hz, the linear mass density of the wire μ is in g/m, and the acceleration due to gravity g is in m/s^2. Note that the measurement accuracy is limited due to heating of the wire, where the uncertainty in the tension is given by:

$$\Delta T = \alpha \rho Y \frac{1}{C\kappa} I^2, \tag{9}$$

where α is the thermal expansion coefficient of the wire material, ρ is the resistivity, Y is Young's modulus, κ is the thermal conductivity, C is a geometrical constant, and I is the driving current.

Appendix III – Capacitance Calculations

i). **No field wires in the wire plane:**

If there are no field shaping wires in the wire plane (only sense wires) the capacitance of the wire is given by Ref.[13] as:

$$C = \frac{2\pi\epsilon_0}{\left(\frac{\pi L}{S}\right) - \ln\left(\frac{2\pi R_s}{S}\right)}, \tag{10}$$

where L is the distance between the wire plane and the cathode plane (the so-called half-gap), S is the separation between adjacent wires, R_s is the radius of the sense wire, and ϵ_0 is the permittivity of free space (8.85 pF/m). For the FDC prototype geometry, L=5 mm, S=10 mm, and R_s=0.01 mm. Plugging these numbers into eq.(10) yields C=8.37 pF/m.

ii). **Field wires in the wire plane:**

If there exist field shaping wires in the sense wire plane, the potentials V_s (sense), V_f (field), and V_c (cathode) each will have three terms, which are due to their own potentials and the potentials induced by the other two planes (see Ref. [14]). These potentials can be represented by the matrix:

$$\begin{pmatrix} V_s \\ V_f \\ V_c \end{pmatrix} = A \begin{pmatrix} \sigma_s \\ \sigma_f \\ \sigma_c \end{pmatrix}, \tag{11}$$

where σ_s, σ_f, and σ_c are the surface charge distributions, and A is the potential coefficient matrix:

$$A = \frac{1}{\epsilon_0} \begin{pmatrix} Z_1 - \frac{S_1}{2\pi}\ln\frac{2\pi R_s}{S_1} & Z_1 - \frac{S_1}{2\pi}\ln 2 & Z_1 \\ Z_1 - \frac{S_1}{2\pi}\ln 2 & Z_1 - \frac{S_1}{2\pi}\ln\frac{2\pi R_f}{S_1} & Z_1 \\ Z_1 & Z_1 & Z_1 \end{pmatrix}. \tag{12}$$

In this expression, Z_1 is the half-gap, S_1 is the separation between the two adjacent sense wires, R_f is the radius of the field wires, and Z_2 is the cathode-to-cathode distance. For the FDC prototype, Z_1=5 mm, S_1=10 mm, R_f=0.07 mm, and Z_2=10 mm. From the matrix for the potentials, charges on the different planes can be written as:

$$\begin{pmatrix} \sigma_s \\ \sigma_f \\ \sigma_c \end{pmatrix} = A^{-1} \begin{pmatrix} V_s \\ V_f \\ V_c \end{pmatrix}, \tag{13}$$

where A^{-1} is the inverse of the matrix A and represents the capacitance matrix. For the FDC prototype this matrix is given by:

$$A^{-1} = \epsilon_0 \begin{pmatrix} 97.0 & -18.1 & -39.4 \\ -18.1 & 137.0 & -59.5 \\ -39.4 & -59.5 & 149.5 \end{pmatrix}. \tag{14}$$

iii) **Strip-to-strip capacitance:**

The capacitance between adjacent strips can be calculated using the equation [4]:

$$C(\mathrm{pF/cm}) = 0.12\frac{t}{w} + 0.09(1+k)\log_{10}\left(1 + \frac{2w}{s} + \frac{w^2}{s^2}\right), \tag{15}$$

where t is the strip thickness, w is the width, s is the separation between strips, and k is the dielectric constant. For the FDC prototype chamber, t=2.0 μm, w=5 mm, s=0.25 mm, and k=3.5 (kapton). From this we find C=1.07 pF/cm. With the calculation repeated for s=0.5 mm and s=0.75 mm, we find C=0.844 pF/cm and C=0.717 pF/cm, respectively.

References

[1] GlueX/Hall D Design Report Version 4, Nov. 2002, pp. 170-171.

[2] ATLAS Technical Design Report Chapter 6, June 1997.

[3] H. Fenker *et al.*, Nucl. Inst. and Meth. A **367**, 285 (1999).

[4] PHENIX Collaboration, see URL
http://www.phenix.bnl.gov/phenix/WWW/muon/phnotes/PN125.

[5] E. Gatti *et al.*, Nucl. Inst. and Meth. **163**, 83 (1979).

[6] G. Charpak and F. Sauli, Nucl. Instr. and Meth. **113**, 381 (1973).

[7] G. Aiken *et al.*, "Design and Performance of the New Cathode Readout Proportional Chambers in LASS", SLAC-PUB-2642, Oct. 1980.

[8] F.J. Barbosa, "A Preamp for the CLAS DC", CLAS-Note 92-003, (1992).

[9] J.A. Kadyk, Nucl. Inst. and Methods A **300**, 436 (1991).

[10] W. Campbell and J. Scialdone, "Outgassing Data for Selecting Spacecraft Materials", NASA internal report RP-1124 Rev. 3 (1993).

[11] S.B. Christo and M.D. Mestayer, "Minimizing Cathode Emission in Drift Chambers", CLAS-Note 92-016, (1992).

[12] GARFIELD has been developed at the University of Mainz by R. Veenhof and revised by M. Guckes and K. Peters. See HELIOS-note 154, (1986).

[13] F. Sauli, "Principles of Operation of Multiwire Proportional and Drift Chambers", CERN internal report 77-09, (1977).

[14] W. Blum and L. Ronaldi, "Particle Detection with Drift Chambers", edited by F. Bounaldi and W. Fabjan, Springer-Verlag, Berlin, (1994).